


ORIGINAL ARTICLE

Open Access



An Integrated Control Framework for Torque Vectoring and Active Suspension System

Jiwei Feng¹, Jinhao Liang^{1*}, Yanbo Lu¹, Weichao Zhuang¹, Dawei Pi², Guodong Yin^{1*} , Liwei Xu¹, Pai Peng¹ and Chaobin Zhou^{1,3}

Abstract

Four-wheel independently driven electric vehicles (FWID-EV) endow a flexible and scalable control framework to improve vehicle performance. This paper integrates the torque vectoring and active suspension system (ASS) to enhance the vehicle's longitudinal and vertical motion control performance. While the nonlinear characteristic of the tire model leads to a relatively heavier computational burden. To facilitate the controller design and ease the load, a half-vehicle dynamics system is built and simplified to the linear-time-varying (LTV) model. Then a model predictive controller is developed by formulating the objective function by comprehensively considering the safety, energy-saving and comfort requirements. The in-wheel motor efficiency and the power loss of tire slip are treated as optimization indices in this work to reduce energy consumption. Finally, the effectiveness of the proposed controller is verified through the rapid-control-prototype (RCP) test. The results demonstrate the enhancement of the energy-saving as well as comfort on the basis of vehicle stability.

Keywords Four-wheel independently driven electric vehicles, Tire nonlinearity, Linear-time-varying (LTV) model, Model predictive control, Rapid control prototype

1 Introduction

Electric vehicles are regarded as a promising solution to deal with the increasing emissions and high energy-efficiency requirements [1–3]. Nowadays, four wheel independently driven electric vehicles (FWID-EVs) with a modular powertrain layout have attracted lots of attention from academic and industrial researchers [4, 5]. Thanks to the simple mechanical structure and short transmission chain, FWID-EVs can quickly respond to

the execution command through the in-wheel motor torque output. Moreover, four independently driven motors provide a considerable enhancement for vehicle stability with a flexible control mode [6–8]. However, the frequent acceleration/deceleration behaviors in urban conditions would affect the vehicle's vertical motion, especially when the torque outputs increase/decrease rapidly. The driver's comfort cannot be guaranteed. To this end, this work integrates the torque vectoring and active suspension system of FWID-EVs focusing on the straight-ahead driving condition. It aims to improve the overall performance on the premise of ensuring vehicle stability.

The four in-wheel motors could generate different torque outputs according to designed torque vectoring strategies [9]. It brings a novel control scheme for the direct yaw moment system rather than only depending on the braking force [10]. By taking the energy efficiency into consideration, the energy consumption can also be reduced [11, 12]. Comprehensively considering the motor

*Correspondence:

Jinhao Liang
ljh19940701@163.com
Guodong Yin
ygd@seu.edu.cn

¹ School of Mechanical Engineering, Southeast University, Nanjing 211189, China

² School of Mechanical Engineering, Nanjing University of Science and Technology, Nanjing 210094, China

³ School of Mechano-Electronic Engineering, Lanzhou University of Technology, Lanzhou 730050, China



efficiency and tire slip energy consumption of FWID-EVs, Zhang et al. [13] propose a torque distribution method based on discrete adaptive sliding control, which effectively reduces the energy loss of vehicles. For the active suspension system, the vehicle heave, pitch, and roll motions can be adjusted with differential active forces [14–16], which is related to ride comfort, road holding stability, and roll prevention.

It is widely accepted that the integration of these subsystems is better to realize holistic control [17, 18]. Many studies focus on longitudinal and lateral integrated control by combining active front wheel steering (AFS) and direct yaw moment control (DYC). An adaptive controller based on a Lyapunov method is employed to coordinate AFS and DYC in Ref. [19]. The adaption law is designed to deal with the uncertain cornering stiffness. A multi-agent system-based control framework is proposed in Ref. [20] to realize the integration of AFS and DYC, in which these subsystems are treated as agents and realize the cooperation by Pareto-optimality theory. Considering the time delay of the vehicle network, a novel H ∞ controller combined with a delay-tolerant linear quadratic regulator is designed in Ref. [21] to improve vehicle stability based on AFS and DYC. Furthermore, to handle the tire nonlinear characteristic, some studies present the Takagi-Sugeno (TS) fuzzy and polytope methods to build the vehicle model, based on which the robust controller is developed. Jin et al. [22] propose a robust state-feedback controller to ensure the vehicle handling performance, in which the T-S fuzzy method is used for the nonlinear Brush tire modeling. Zhang et al. [23, 24] adopt the polytope to describe the uncertainties in the model. A robust gain-scheduled controller is designed to enhance the vehicle's lateral stability. It is worth mentioning that an inappropriate Lyapunov function would lead to being conservative of robust controller when handling the tire's nonlinear characteristic [16, 25].

In addition to the vehicle longitudinal and lateral motion control, some studies also integrate vertical motion. Zhao et al. [17] develop a hierarchical framework to coordinate AFS, ASS and DYC, thereby improving the overall performance. A trigger mechanism is established to decide the working regions of different subsystems based on the tire reserve forces. Hussein et al. [18] propose a high-order sliding model method to realize a global chassis control. The results show the effectiveness of enhancing the vehicle stability and ride comfort. Qin et al. [26] investigate the couplings between the dynamic vibration-absorbing structures and in-wheel motors. A particle optimization method is adopted to enhance the vertical dynamics performance. Nevertheless, the energy-saving is seldom considered in the integration of these subsystems. The researches in Refs. [1, 27, 28] demonstrate that energy consumption can be reduced

through a reasonable torque vectoring strategy, as well as improving the vehicle stability.

Meanwhile, model predictive control (MPC) has been increasingly used in the vehicle dynamics control [29, 30]. The MPC does not adopt a constant global optimization target, but repeatedly optimizes online in a rolling method to obtain a global sub-optimal solution. It has strong adaptability to complex and changeable driving environments, and can meet the needs of real-time online optimization control under multi-objective compound constraints. Hence, a model predictive controller is proposed in this paper to integrate the torque vectoring and active suspension system by comprehensively considering safety, energy-saving and comfort. A non-linear model predictive controller is applied to improve the stability of distributed drive electric vehicles under critical driving scenarios [29]. The experiments on the snowy road validate the feasibility. The path-tracking problem is transformed into a standard MPC optimization problem in Ref. [30]. Multi-constraints are also considered in the solver.

The main contributions of this paper are as follows. First, a half-vehicle dynamics model is employed to describe the vehicle's longitudinal and vertical motions, in which the nonlinear tire dynamics is described by an LTV model. It facilitates the controller design and reduces the computational load. Then, a model predictive controller is developed by optimizing the multi-objectives, including energy-saving, vehicle safety, and comfort. The RCP experiments are conducted to validate the effectiveness of the proposed method.

The remainder of this paper is organized as follows. A half-vehicle system combined with a tire dynamics model is built in Section 2. In Section 3, the MPC controller and the test bench are discussed. The optimization objective functions are given in detail. Section 4 shows the test results of the proposed controller. Finally, Section 5 presents the conclusion.

2 Vehicle System Modeling

This work focuses on vehicle control for the straight-ahead driving condition. Hence, the vehicle's longitudinal motion and vertical motion are investigated in this section. A half-vehicle model is established. Moreover, the nonlinear characteristic of the tire model is fully considered and simplified to facilitate the controller design.

2.1 Wheel Dynamics

Considering the effect of vehicle vertical motion on the straight line driving, the vehicle longitudinal dynamics model can be expressed as:

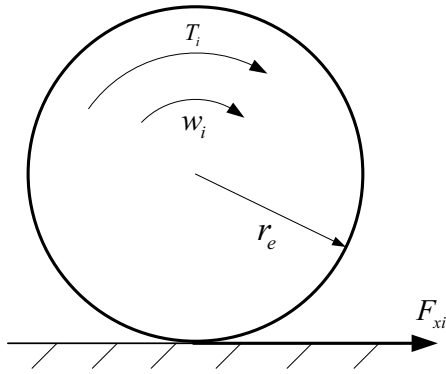


Figure 1 Wheel dynamics model

$$m\dot{V}_x + m_s V_z \dot{\theta} = \sum_{i=f,r} F_{xi}, \tag{1}$$

where m and m_s represent the total mass and sprung mass of the vehicle, respectively. V_x and V_z are the vehicle longitudinal and vertical velocities. θ is the vehicle pitch angle. F_{xf} and F_{xr} denote the longitudinal forces of the front and rear tires, respectively, which are generated by the torque inputs of the in-wheel motors. Furthermore, the wheel dynamics as shown in Figure 1 is given by:

$$J_w \dot{w}_i = T_{wi} - r_e F_{xi}, \tag{2}$$

where J_w and r_e are the inertia moment and rolling radius of wheel, respectively. T_{wi} is the torque input of the in-wheel motor i . w_i is the rotational speed of the wheel i , $i = f, r$; f represents the front tire, and r represents the rear tire. When the vehicle runs in the linear region, the tire longitudinal force can be represented by:

$$F_{xi} = K_{xi} \lambda_i, \tag{3}$$

where K_{xi} is the tire longitudinal stiffness, which is related with the vertical load, tire type and tire pressure, etc. λ_i is the tire longitudinal slip ratio. It can be further expressed as:

$$\lambda_i = \frac{w_i r_e - V_x}{V_x}. \tag{4}$$

For Eq. (3), when the vehicle is in the nonlinear region, it would be invalid if using the longitudinal tire stiffness K_{xi} obtained by the linear state. A conventional method is to adopt the tire fitting formulas and calculate the tire force in real time [31]. This can guarantee the model's accuracy. However, the tire force is directly employed in the system. Due to the strong nonlinearity, it would cause a large computational burden for the optimization. Hence, a modified tire longitudinal stiffness K'_{xi} is defined in this work to ensure accuracy while reducing the computational burden through the linearization method. The tire longitudinal

force F_{xi} is calculated by the Magic formula. Then the modified tire longitudinal stiffness K'_{xi} is calculated by Eq. (3) in real-time and presented by a time-varying parameter. The K'_{xi} would change according to different driving conditions. By introducing the modified parameter K'_{xi} into the Eq. (2), the wheel dynamics can be rewritten as:

$$\dot{\lambda}_i = -\frac{r_e^2}{J_w V_x} K'_{xi} \lambda_i + \frac{r_e}{J_w V_x} T_{wi}. \tag{5}$$

The Magic formula [32] fitting the tire longitudinal force is given by:

$$F_{xi} = \mu F_{zi} \sin \left\{ C_x \arctan \left[\frac{B_x \lambda_i - D_x (B_x \lambda_i - B_x \arctan(\lambda_i))}{D_x} \right] \right\}, \tag{6}$$

where μ is the road-tire friction coefficient. B_x , C_x and D_x are obtained through the parameter fitting method. F_{zi} is the vertical load of the i -wheel, which can be calculated by:

$$F_{zf} = \frac{mg}{2} \left[\frac{l_r}{l_f + l_r} - \frac{h}{(l_f + l_r)g} a_x \right], \tag{7}$$

$$F_{zr} = \frac{mg}{2} \left[\frac{l_f}{l_f + l_r} + \frac{h}{(l_f + l_r)g} a_x \right], \tag{8}$$

where l_f and l_r are the distances from the vehicle centre of gravity (CoG) to the front and rear axles. h and a_x are the height of CoG and vehicle longitudinal acceleration, respectively. g is the gravitational acceleration. To show the accuracy of the Magic formula, the fitting tire longitudinal forces under different vertical loads (i.e., 2.1 kN, 6.1 kN and 10.1 kN) are compared with the real test data. The detailed results are shown in Figure 2. During the straight driving condition, the tire slip angle α is 0.

From the test results, it can be seen that the fitting tire longitudinal force is closely approaching the test data. Consequently, the tire longitudinal force F_{xi} is obtained through the Magic formula in this work. Here, the tire test data are

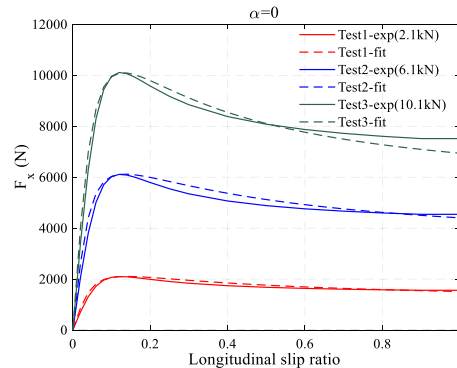


Figure 2 Tire longitudinal force fitting results

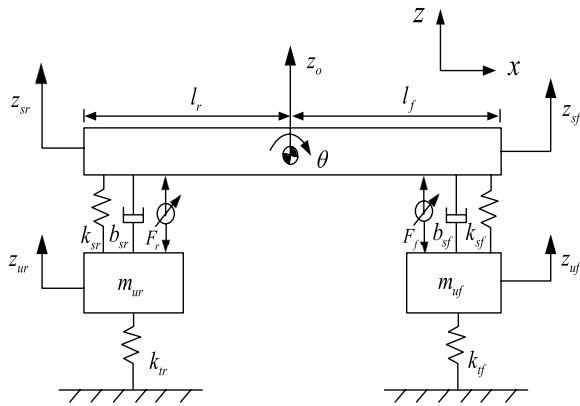


Figure 3 4-DoF vehicle vertical dynamics model

collected from a high-fidelity vehicle model (CarSim). Then the modified tire longitudinal stiffness K'_{xi} is obtained in real-time based on Eq. (3). Eq. (1) can be expressed as:

$$m\dot{V}_x + m_s V_z \dot{\theta} = K'_{xf} \lambda_f + K'_{xr} \lambda_r. \tag{9}$$

2.2 Vehicle Vertical Dynamics

The vehicle would have obvious heave and pitch motions when existing frequent acceleration/deceleration behaviors. To describe the vehicle vertical motion, a 4-degree-of-freedom (4-DoF) half-vehicle active suspension system as shown in Figure 3 is used to establish the vehicle vertical dynamics model. F_f and F_r are active suspension forces, which are generated by the actuators. The roll motion is ignored due to the straight line driving. With the assumption of a small pitch angle. The heave motion of the sprung mass and unsprung mass can be represented by:

$$m_s (\ddot{z}_o - V_x \dot{\theta}) = \begin{bmatrix} -k_{sf}(z_{sf} - z_{uf}) - b_{sf}(\dot{z}_{sf} - \dot{z}_{uf}) + F_f \\ -k_{sr}(z_{sr} - z_{ur}) - b_{sr}(\dot{z}_{sr} - \dot{z}_{ur}) + F_r \end{bmatrix}, \tag{10}$$

$$m_{uf} \ddot{z}_{uf} = \begin{bmatrix} k_{sf}(z_{sf} - z_{uf}) + b_{sf}(\dot{z}_{sf} - \dot{z}_{uf}) \\ -F_f - k_{tf} z_{uf} \end{bmatrix}, \tag{11}$$

$$m_{ur} \ddot{z}_{ur} = \begin{bmatrix} k_{sr}(z_{sr} - z_{ur}) + b_{sr}(\dot{z}_{sr} - \dot{z}_{ur}) \\ -F_r - k_{tr} z_{ur} \end{bmatrix}. \tag{12}$$

It should be noted that the road excitation is not considered in this study. z_o is the vertical displacement of the vehicle CoG. k_{sf} and k_{sr} are the equivalent stiffness of the front and rear suspensions, respectively. b_{sf} and b_{sr} are the equivalent damping of the front and rear suspensions. k_{tf} and k_{tr} are the equivalent stiffness of the front and rear wheels, respectively. z_{sf} and z_{sr} are the vertical displacements of the front and rear sprung mass. z_{uf} and z_{ur} are the vertical displacements of the front and rear unsprung mass, respectively. F_f and F_r are the active force inputs of the front and rear suspensions, respectively. m_{uf} and m_{ur} are the unsprung mass of the front and rear wheels, respectively. Furthermore, the vertical displacements of the front and rear sprung mass can be expressed as:

$$z_{sf} = z_o - l_f \theta, \tag{13}$$

$$z_{sr} = z_o + l_r \theta. \tag{14}$$

The pitch motion of the suspension system can be described by

$$I_y \ddot{\theta} = -l_f \mathfrak{R}_f + l_r \mathfrak{R}_r, \tag{15}$$

where I_y is the vehicle inertia moment around the y-axis.

$$\mathfrak{R}_f = -k_{sf}(z_{sf} - z_{uf}) - b_{sf}(\dot{z}_{sf} - \dot{z}_{uf}) + F_f, \tag{16}$$

$$\mathfrak{R}_r = -k_{sr}(z_{sr} - z_{ur}) - b_{sr}(\dot{z}_{sr} - \dot{z}_{ur}) + F_r. \tag{17}$$

Combining Eqs. (1)–(17), the vehicle system model for the straight-ahead driving condition is given by

$$\dot{\mathbf{x}}(t) = \mathbf{A}\mathbf{x}(t) + \mathbf{B}\mathbf{u}(t), \tag{18}$$

where $\mathbf{x} = [V_x, \lambda_f, \lambda_r, \theta, \dot{\theta}, z_o, \dot{z}_o, z_{uf}, z_{ur}, \dot{z}_{uf}, \dot{z}_{ur}]^T$, $\mathbf{u} = [T_f, T_r, F_f, F_r]^T$,

$$\mathbf{A} = \begin{bmatrix} \frac{K'_{xf}}{m} & 0 & \frac{K'_{xr}}{m} & 0 & -V_z & 0 & 0 & 0 & 0 & 0 & 0 & 0 \\ 0 & a_{22} & 0 & 0 & 0 & 0 & 0 & 0 & 0 & 0 & 0 & 0 \\ 0 & 0 & a_{33} & 0 & 0 & 0 & 0 & 0 & 0 & 0 & 0 & 0 \\ 0 & 0 & 0 & 0 & 1 & 0 & 0 & 0 & 0 & 0 & 0 & 0 \\ 0 & 0 & 0 & a_{54} & a_{55} & a_{56} & a_{57} & a_{58} & a_{59} & a_{5,10} & a_{5,11} & 0 \\ 0 & 0 & 0 & 0 & 0 & 0 & 1 & 0 & 0 & 0 & 0 & 0 \\ 0 & 0 & 0 & a_{74} & a_{75} & a_{76} & a_{77} & a_{78} & a_{79} & a_{7,10} & a_{7,11} & 0 \\ 0 & 0 & 0 & 0 & 0 & 0 & 0 & 0 & 0 & 1 & 0 & 0 \\ 0 & 0 & 0 & 0 & 0 & 0 & 0 & 0 & 0 & 0 & 0 & 1 \\ 0 & 0 & 0 & a_{10,4} & a_{10,5} & a_{10,6} & a_{10,7} & a_{10,8} & 0 & a_{10,10} & 0 & 0 \\ 0 & 0 & 0 & a_{11,4} & a_{11,5} & a_{11,6} & a_{11,7} & 0 & a_{11,9} & 0 & a_{11,11} & 0 \end{bmatrix}_{11 \times 11},$$

$$B = \begin{bmatrix} 0 & \frac{r_e}{J_w * V_x} & 0 & 0 & 0 & 0 & 0 & 0 & 0 \\ 0 & 0 & \frac{r_e}{J_w * V_x} & 0 & 0 & 0 & 0 & 0 & 0 \\ 0 & 0 & 0 & 0 & -\frac{l_f}{I_y} & 0 & \frac{1}{m_s} & 0 & 0 & -\frac{1}{m_{uf}} & 0 \\ 0 & 0 & 0 & 0 & -\frac{l_r}{I_y} & 0 & \frac{1}{m_s} & 0 & 0 & 0 & -\frac{1}{m_{ur}} \end{bmatrix}^T, \quad 4 \times 11$$

$$a_{22} = -K'_{sf} * r_e * r_e / (J_w * V_x), a_{33} = -K'_{xr} * r_e * r_e / (J_w * V_x),$$

$$a_{54} = (-k_{sf} * l_f * l_f - k_{sr} * l_r * l_r) / I_y,$$

$$a_{56} = (k_{sf} * l_f - k_{sr} * l_r) / I_y,$$

$$a_{55} = (-b_{sf} * l_f * l_f - b_{sr} * l_r * l_r) / I_y$$

$$a_{57} = (b_{sf} * l_f - b_{sr} * l_r) / I_y, a_{58} = -k_{sf} * l_f / I_y,$$

$$a_{59} = k_{sr} * l_r / I_y, a_{5,10} = -b_{sf} * l_f / I_y, a_{5,11} = b_{sr} * l_r / I_y,$$

$$a_{74} = (k_{sf} * l_f - k_{sr} * l_r) / m_s,$$

$$a_{75} = (b_{sf} * l_f - b_{sr} * l_r + m_s * V_x) / m_s,$$

$$a_{76} = (-k_{sf} - k_{sr}) / m_s, a_{77} = (-b_{sf} - b_{sr}) / m_s,$$

$$a_{78} = k_{sf} / m_s, a_{79} = k_{sr} / m_s, a_{7,10} = b_{sf} / m_s, a_{7,11} = b_{sr} / m_s,$$

$$a_{10,4} = -k_{sf} * l_f / m_{uf}, a_{10,5} = -b_{sf} * l_f / m_{uf},$$

$$a_{10,6} = k_{sf} / m_{uf}, a_{10,7} = b_{sf} / m_{uf}$$

$$a_{10,8} = (-k_{tf} - k_{sf}) / m_{uf}, a_{10,10} = -b_{sf} / m_{uf},$$

$$a_{11,4} = k_{sr} * l_r / m_{ur}, a_{11,5} = b_{sr} * l_r / m_{ur}, a_{11,6} = k_{sr} / m_{ur},$$

$$a_{11,7} = b_{sr} / m_{ur}, a_{11,9} = (-k_{tr} - k_{sr}) / m_{ur},$$

$$a_{11,11} = -b_{sr} / m_{ur}.$$

It could be found that the model (18) is a continuous-time nonlinear system. The parameter matrices A and B exist time-varying state variables, including longitudinal velocity V_x and modified tire longitudinal stiffness K'_{xi} . Here, to facilitate the model predictive control (MPC) design and reduce the computational burden. A linear-time-varying (LTV) discrete model is established. The state variables in the parameter matrices are treated as a constant during the sampling time, which would update at different sampling time. The sampling time is given by Γ . Then based on the Euler method, the continuous system (18) at time step k can be discretized as:

$$x(k + 1) = A_c x(k) + B_c u(k), \quad (19)$$

where $x(k)$ and $u(k)$ represent system states and inputs at time step k , respectively.

$$\begin{cases} A_c = e^{A\Gamma}, \\ B_c = \int_{k\Gamma}^{(k+1)\Gamma} e^{A[(k+1)\Gamma-t]} B dt. \end{cases} \quad (20)$$

The handling of model linearization and discretization simplifies the system and facilitates the controller design [33]. Meanwhile, the tire characteristic can also be guaranteed.

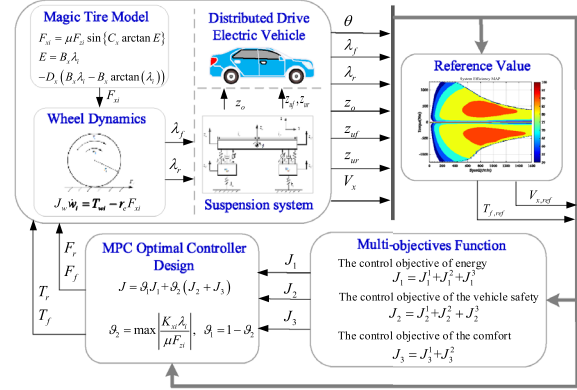


Figure 4 Schematic integrated control framework for torque vectoring and active suspension system

3 Optimal Control Design

The schematic integrated control framework for torque vectoring and active suspension system is shown in Figure 4. It includes the wheel dynamics model, nonlinear tire model, 4-DoF vehicle vertical dynamics model, reference model and MPC optimal controller. The MPC controller is proposed to realize the integrated control of vehicle longitudinal and vertical motions. A combination of multi-performance indices, including energy saving, vehicle safety, and comfort, are considered during the controller design. The relaxation factors are introduced to dynamically modulate the weight coefficients of different control objectives. Furthermore, to better verify the controller control effect, the rapid-control-prototype test bench is also described.

3.1 Multi-objectives Function

The control objective of energy saving can be represented as follows:

$$J_1 = J_1^1 + J_1^2 + J_1^3, \quad (21)$$

where

$$J_1^1 = \sum_{t=1}^{N_p-1} \|T_f(k+t|k) - T_{f,ref}\|_{Q_1}^2, \quad (22)$$

$$J_1^2 = \sum_{t=1}^{N_p-1} \|F_{x,i} \lambda_i V_x\|_{Q_2}^2, \quad (23)$$

$$J_1^3 = \sum_{t=1}^{N_p-1} \left(\|T_i(k+t|k)\|_{R_1}^2 + \|F_i(k+t|k)\|_{R_2}^2 \right), \quad (24)$$

where $T_i = [T_f \ T_r]^T$, $F_i = [F_f \ F_r]^T$, $Q_1 \in \mathbb{R}^{1 \times 1}$, $Q_2 \in \mathbb{R}^{2 \times 2}$, $R_1 \in \mathbb{R}^{2 \times 2}$, and $R_2 \in \mathbb{R}^{2 \times 2}$ are the positive

diagonal matrices, which represent the weight parameters. N_p is the predictive horizon. In this work, the predictive horizon is equal to the control horizon. $T_{f,ref}$ is the reference torque inputs of the front in-wheel motor. The optimization objective (21) is a combination of different energy consumption. The cost function (22) considers energy saving through improving the motor efficiency, based on optimizing the torque inputs. To reduce energy consumption, the selection principle of the reference torque inputs is to provide a high-efficiency zone for in-wheel motors. The efficiency map for the in-wheel motor is given in Figure 5, in which the test data is collected from a Protean PD-18 in-wheel motor. A wheel speed-motor efficiency mapping table is designed to obtain the reference torque inputs $T_{f,ref}$ by matching the wheel speed. Under some specific driving conditions, the torque inputs of the in-wheel motors may deviate from the high-efficiency zone. In this case, the energy consumption would be reduced if matching the high-efficiency zone for some in-wheel motors first. Simultaneously when rear tires approach the saturation state, a small lateral force could cause the vehicle sideslip. Considering the longitudinal stability control, the in-wheel motors of the front axle would satisfy the high-efficiency state in priority. The cost function (23) is the power loss of the longitudinal slip for the front and rear tires. It can be further represented by:

$$J_1^2 = \sum_{t=1}^{N_p-1} \left\| K'_{xi} \lambda_i^2(k+t|k) V_x(k+t|k) \right\|_{Q_2}^2. \quad (25)$$

For Eq. (24), it denotes the energy consumption caused by the actuators. The control objective of the vehicle safety can be expressed by

$$J_2 = J_2^1 + J_2^2 + J_2^3, \quad (26)$$

where

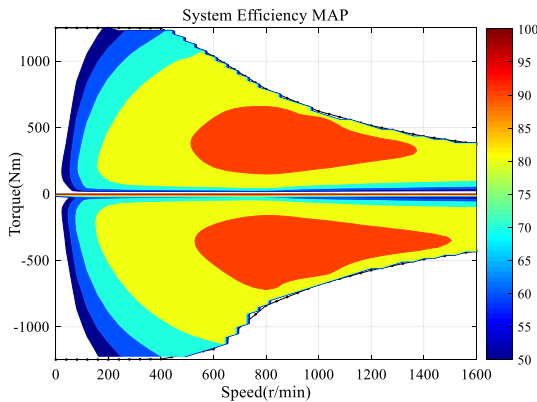


Figure 5 Efficiency map of in-wheel motors

$$J_2^1 = \sum_{t=1}^{N_p-1} \left\| \lambda_i(k+t|k) \right\|_{W_1}^2, \quad (27)$$

$$J_2^2 = \sum_{t=1}^{N_p-1} \left\| z_{si}(k+t|k) - z_{ui}(k+t|k) \right\|_{W_2}^2, \quad (28)$$

$$J_2^3 = \sum_{t=1}^{N_p-1} \left\| V_x(t+k|k) - V_{x,ref} \right\|_{W_3}^2, \quad (29)$$

where $\lambda_i = [\lambda_f \ \lambda_r]^T$, $z_{si} = [z_{sf} \ z_{sr}]^T$, $z_{ui} = [z_{uf} \ z_{ur}]^T$. $W_1 \in \mathbb{R}^{2 \times 2}$, $W_2 \in \mathbb{R}^{2 \times 2}$ and $W_3 \in \mathbb{R}^{1 \times 1}$ are the positive diagonal matrices. The cost function (27) aims to minimize the tire slip ratio and improve the vehicle safety. In addition, as designed in the cost function (22), the front in-wheel motors are endowed with the high priority to match the efficiency zone, thereby guaranteeing the vehicle longitudinal stability. Furthermore, to enhance the vehicle vertical safety, the cost function (28) is presented by a soft constraint to depress the suspension deflections, which should also satisfy the hard constraint [34] shown as follows:

$$|z_{si} - z_{ui}| \leq \rho z_{max}, \quad (30)$$

where $\rho = [1 \ 1]^T$, z_{max} is the permitted maximum value of the suspension deflection. As for the cost function (29), it represents the speed control requirement of drivers. When the vehicle speed is lower than the drivers' intention, drivers would have an acceleration behavior and increase the torque inputs. Conversely, drives have a deceleration behavior. Therefore, the weight parameter W_3 has a bigger value to follow the reference speed and satisfy the drivers' demand. The control objective of the comfort is expressed as follows:

$$J_3 = J_3^1 + J_3^2, \quad (31)$$

where

$$J_3^1 = \sum_{t=1}^{N_p-1} \left\| \ddot{z}_o(t+k|k) \right\|_{P_1}^2 = \sum_{t=1}^{N_p-1} \left\| Cx(t+k|k) \right\|_{P_1}^2, \quad (32)$$

where $C = [0 \ 0 \ 0 \ a_{74} \ a_{75} \ a_{76} \ a_{77} \ a_{78} \ a_{79} \ a_{7,10} \ a_{7,11}]$,

$$J_3^2 = \sum_{t=1}^{N_p-1} \left(\left\| \theta(t+k|k) \right\|_{P_2}^2 + \left\| z_o(t+k|k) \right\|_{P_3}^2 \right). \quad (33)$$

Here, the vertical displacement and acceleration of vehicle CoG, and pitch angle are employed to quantify

and describe the ride comfort. The cost functions (32) and (33) aim to suppress the vehicle heave motion and vertical motion, thereby improving the drivers' comfort. Combining Eqs. (21)–(33), the global optimization objective function is expressed as follows:

$$J = \vartheta_1 J_1 + \vartheta_2 (J_2 + J_3), \tag{34}$$

where ϑ_1 and ϑ_2 are relaxation factors to balance the performance indices between energy-saving, ride comfort and safety control. The vehicle safety should be put in the first place during some extreme conditions. In this work, the slip ratio λ_i is selected to evaluate the vehicle longitudinal stability, which also satisfies Eq. (35):

$$F_{xi} = K_{xi}' \lambda_i \leq \mu F_{zi}. \tag{35}$$

To guarantee the vehicle stability when the available tire force is small, the relaxation factors is calculated by:

$$\begin{cases} \vartheta_2 = \max \left| \frac{K_{xi} \lambda_i}{\mu F_{zi}} \right|, \\ \vartheta_1 = 1 - \vartheta_2. \end{cases} \tag{36}$$

3.2 Rapid-Control-Prototype (RCP) Test

The optimal problem is represented by:

$$\min_u J. \tag{37}$$

Subject to $u_{\min} \leq u \leq u_{\max}$ and hard constraint (30).

The rapid-control-prototype (RCP) test bench as shown in Figure 6 is built to validate the effectiveness of the proposed control method. It includes a real-time simulation system based on NI-PXI, a high-speed solution system based on dSPACE, and a high-fidelity vehicle system based on CarSim. In the RCP system established in this paper, a high-fidelity vehicle dynamic modeling business software (CarSim) is embedded into a real-time simulator (NI-PXI system). The optimal control solver is

downloaded to the dSPACE-1401(900 MHz, 16 MByte) and running in real time. Based on the vehicle state feedback from the CarSim, the dSPACE can calculate the optimal inputs, which would be sent to the NI-PXI system and executed by the vehicle. The CAN bus is adopted to realize the data transmission. To avoid potential system disturbances, the first sequence of the optimal inputs is employed in the system. In addition, the updating states in the LTV model (18) would also transmit to the controller at each sampling time.

4 Test Results

This section validates the effectiveness of the proposed controller through the RCP test. The Economic Commission for Europe (ECE) is chosen as the test condition. To show the control performance visually, a part of the velocity profile for the ECE elementary urban cycle is adopted to test the stability and energy-saving with the proposed torque vectoring strategy, while the ECE extra-urban driving cycle with frequent acceleration behavior is to test the ride comfort with the proposed active suspension system. The vehicle parameters used in this work are given in Table 1. The RCP has been conducted through the GRAMPC optimization solver [35], which is adapted to the nonlinear MPC and can be employed in the dSPACE through code generation technology. In addition, the LQR controller is set as a comparison test in this work. The road-tire friction coefficient is set by 0.5. The control horizon is 3 and the prediction horizon is 5.

4.1 ECE Elementary Urban Cycle

The simulation results under the ECE elementary urban cycle are shown in Figure 7. Figure 7(a) shows the torque inputs of the in-wheel motors. Figure 7(b) is the velocity tracking performance with the different

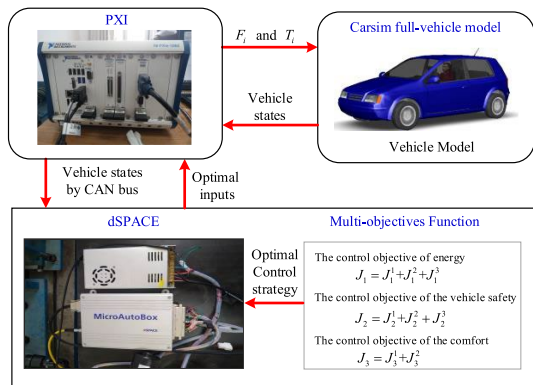


Figure 6 RCP test bench

Table 1 Vehicle parameters

Parameter description	Value
Vehicle total mass m (kg)	1558
Sprung mass m_s (kg)	1274
Unsprung mass at each corner of the chassis m_u (kg)	71
Height from CG to roll center h_s (m)	0.54
Inertia moment around the y-axis I_y (kg·m ²)	1523
Distance between CG and front axle l_f (m)	1.016
Distance between CG and rear axle l_r (m)	1.562
Front suspension spring stiffness k_{sF} (N/m)	27000
Rear suspension spring stiffness k_{sR} (N/m)	30000
Suspension damping stiffness b_{sj} (N·s/m)	1856
Tire vertical stiffness k_{ti} (N/m)	228000

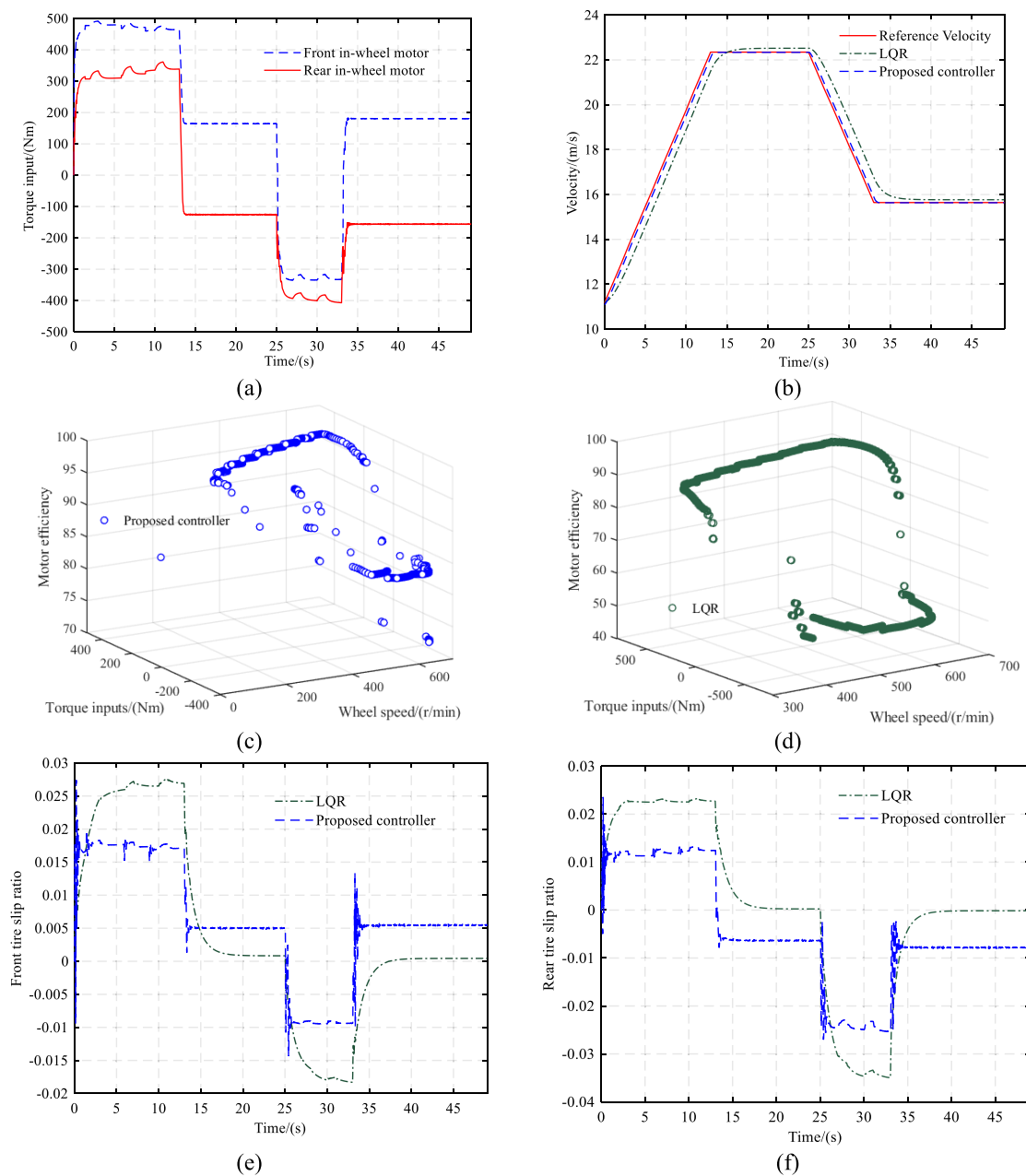


Figure 7 The simulation results under the ECE elementary urban cycle: (a) Torque inputs of in-wheel motors, (b) Vehicle velocity, (c) Motor efficiency with the proposed controller, (d) Motor efficiency with LQR controller, (e) Front tire slip ratio, (f) Rear tire slip ratio

strategies. It can be seen that the vehicle can track the reference velocities closely with the proposed control strategy, while there exists obvious overshoots and undershoots with the LQR controller. The maximum tracking errors with the two strategies are 0.05 m/s and 1 m/s, respectively. This is because the tire longitudinal stiffness is a constant value when calculating the feedback control law for the LQR. However, the accurate time-varying tire longitudinal stiffness is obtained with

the proposed controller in real time and used to calculate the optimized torque inputs.

The efficiency maps of the front in-wheel motor with different strategies are given in Figure 7(c) and (d). It is clear that with the proposed control strategy, the in-wheel motor can work in a relatively high-efficiency zone, which basically maintains a level of 85%–95%. The motor efficiency of the LQR controller keeps low in some regions, which is between 40% and 55%. This

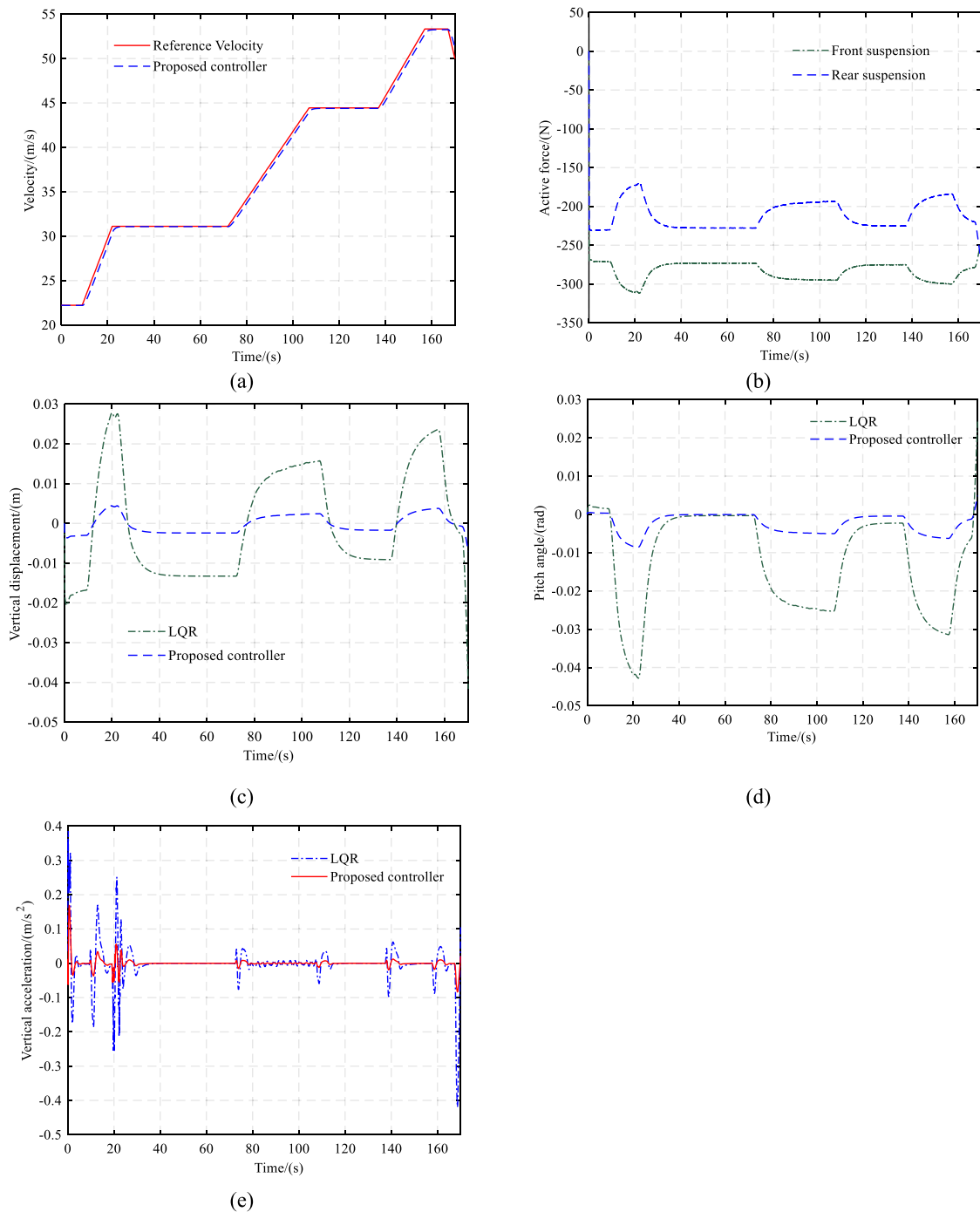


Figure 8 The simulation results under the ECE extra-urban driving cycle with frequent acceleration behavior: (a) Vehicle velocity, (b) Active suspension force inputs, (c) Vertical displacements, (d) Vehicle pitch angle, (e) Vehicle vertical acceleration

proves that the proposed torque vectoring strategy can improve energy efficiency. It could be noted that the motor efficiency reduces when the torque input of the front wheel reaches $-300 \text{ N}\cdot\text{m}$ (i.e., 25–32 s) with the proposed controller. This can be attributed to the

velocity tracking. As shown in Figure 7(b), the reference velocity drops quickly during 25–32 s. Hence, the torque inputs are reduced to track the reference velocities, which causes a lower motor efficiency zone.

Figure 7(e) and (f) are the longitudinal slip ratio of the front and rear tires. The tire slip ratio has a smaller value with the proposed controller compared to the LQR. This means that the vehicle can run in a more stable state with less power loss of the longitudinal slip. Some fluctuations can be seen in the tire slip ratio. This is because the MPC controller is a real-time optimization solver. External disturbances, such as time delays in the data transmission, would have an effect on the optimization results, thereby affecting the system states. According to these comparative test results, it can be concluded that the proposed torque vectoring can effectively guarantee the velocity tracking performance while ensuring vehicle stability and energy efficiency.

4.2 ECE Extra-Urban Driving Cycle

The ECE extra-urban driving cycle with frequent acceleration behavior is employed to value ride comfort with different strategies. Figure 8 shows the test results. As shown in Figure 8(a), it can be found that the vehicle velocity is close to the reference value with the proposed controller. Figure 8(b) represents the active force inputs of the front and rear suspensions, respectively. The vertical displacements of vehicle CoG with different controllers are given in Figure 8(c). The maximum vertical displacements are 0.028 and 0.005 m, respectively. This demonstrates that the vehicle has a smaller displacement with the proposed strategy, thereby improving the driver's comfort. Meanwhile, it can be seen that when a vehicle has a positive displacement, the active suspension generates a negative force to reduce the vertical deformation.

Figure 8(d) illustrates the vehicle pitch angle. The maximum pitch angle with the proposed controller can be reduced by 78% compared to the LQR controller. The differential active suspension forces as shown in Figure 8(b) significantly depress the pitch angle. It can relieve the driver's discomfort when suffering frequent acceleration/deceleration behavior. The vertical acceleration of vehicle CoG is shown in Figure 8(e). It is clear that the vehicle has a better performance to improve the vehicle's vertical motion. These prove that the proposed control strategy is effective for the vehicle vertical dynamics control.

5 Conclusions

- (1) This paper applies the LTV-MPC controller to integrate the vehicle torque vectoring and active suspension system for the straight-ahead driving condition. The vehicle dynamics model

considers the nonlinear characteristic of the tire. Then the fitting magic formula validated by the experimental data is used to obtain the tire longitudinal stiffness in real-time, based on which updating the system model parameters. To satisfy the tracking performance of the system states while guaranteeing vehicle safety, energy-saving and comfort, a combination of the optimization functions is formulated. Rapid control prototype tests are conducted to verify the proposed control strategy. The control effect of the LQR controller is compared with that of the proposed control strategy. The results show that compared with the LQR control strategy, the proposed control strategy can improve motor efficiency by nearly 73%.

- (2) Two types of ECE test results show that the proposed controller can effectively guarantee the velocity tracking performance while ensuring vehicle stability and improving energy efficiency and comfort. In the future, the vehicle steering behavior is also expected to be combined in the system.

Acknowledgements

Not applicable.

Authors' Contributions

JF, JL, WZ, GY, and LX were in charge of the whole trial; JF wrote the manuscript; YL, DP, PP, and CZ assisted with sampling and laboratory analyses. All authors read and approved the final manuscript.

Funding

Supported by National Natural Science Foundation of China (Grant Nos. 51975118, 52025121), Foundation of State Key Laboratory of Automotive Simulation and Control of China (Grant No. 20210104), Foundation of State Key Laboratory of Automobile Safety and Energy Saving of China (Grant No. KFZ2201), Special Fund of Jiangsu Province for the Transformation of Scientific and Technological Achievements of China (Grant No. BA2021023).

Availability of Data and Materials

The datasets supporting the conclusions of this article are included within the article.

Declarations

Ethics Approval and Consent to Participate

Not applicable.

Consent for Publication

Not applicable.

Competing Interests

The authors declare no competing financial interests.

Received: 5 March 2023 Revised: 29 November 2023 Accepted: 19 January 2024

Published online: 22 February 2024

References

- [1] X Hu, H Chen, Z Li, et al. An energy-saving torque vectoring control strategy for electric vehicles considering handling stability under extreme conditions. *IEEE Transactions on Vehicular Technology*, 2020, 69(10): 10787–10796.
- [2] R de Castro, R E Araujo, D Freitas. Wheel slip control of EVs based on sliding mode technique with conditional integrators. *IEEE Transactions on Industrial Electronics*, 2012, 60(8): 3256–3271.
- [3] H Dong, W Zhuang, G Yin, et al. Energy-optimal braking control using a double-layer scheme for trajectory planning and tracking of connected electric vehicles. *Chinese Journal of Mechanical Engineering*, 2021, 34: 83.
- [4] D Zhang, G Liu, H Zhou, et al. Adaptive sliding mode fault-tolerant coordination control for four-wheel independently driven electric vehicles. *IEEE Transactions on Industrial Electronics*, 2018, 65(11): 9090–9100.
- [5] C Hu, R Wang, F Yan. Integral sliding mode-based composite nonlinear feedback control for path following of four-wheel independently actuated autonomous vehicles. *IEEE Transactions on Transportation Electrification*, 2016, 2(2): 221–230.
- [6] C Geng, L Mostefai, M Denai, et al. Direct yaw-moment control of an in-wheel-motored electric vehicle based on body slip angle fuzzy observer. *IEEE Transactions on Industrial Electronics*, 2009, 56(5): 1411–1419.
- [7] J Hu, Y Wang, H Fujimoto, et al. Robust yaw stability control for in-wheel motor electric vehicles. *IEEE/ASME Transactions on Mechatronics*, 2017, 22(3): 1360–1370.
- [8] J Wu, J Zhang, B Nie, et al. Adaptive control of PMSM servo system for steering-by-wire system with disturbances observation. *IEEE Transactions on Transportation Electrification*, 2022, 8(2): 2015–2028.
- [9] A Wong, D Kasinathan, A Khajepour, et al. Integrated torque vectoring and power management framework for electric vehicles. *Control Engineering Practice*, 2016, 48: 22–36.
- [10] Y Chen, J K Hedrick, K Guo. A novel direct yaw moment controller for in-wheel motor electric vehicles. *Vehicle System Dynamics*, 2013, 51(6): 925–942.
- [11] J Gu, M Ouyang, D Lu, et al. Energy efficiency optimization of electric vehicle driven by in-wheel motors. *International Journal of Automotive Technology*, 2013, 14: 763–772.
- [12] B Zhao, N Xu, H Chen, et al. Design and experimental evaluations on energy-efficient control for 4WIMD-EVs considering tire slip energy. *IEEE Transactions on Vehicular Technology*, 2020, 69(12): 14631–14644.
- [13] H Zhang, C Zhou, C Wang, et al. An energy efficient control strategy for electric vehicle driven by in-wheel-motors based on discrete adaptive sliding mode control. *Chinese Journal of Mechanical Engineering*, 2023, 36: 58.
- [14] W Li, Z Xie, Y Cao, et al. Sampled-data asynchronous fuzzy output feedback control for active suspension systems in restricted frequency domain. *IEEE/CAA Journal of Automatica Sinica*, 2020, 8(5): 1052–1066.
- [15] M Yu, C Arana, S A Evangelou, et al. Parallel active link suspension: A quarter-car experimental study. *IEEE/ASME Transactions on Mechatronics*, 2018, 23(5): 2066–2077.
- [16] H Du, N Zhang. Fuzzy control for nonlinear uncertain electrohydraulic active suspensions with input constraint. *IEEE Transactions on Fuzzy Systems*, 2008, 17(2): 343–356.
- [17] H Termous, H Shraim, R Talj, et al. Coordinated control strategies for active steering, differential braking and active suspension for vehicle stability, handling and safety improvement. *Vehicle System Dynamics*, 2019, 57(10): 1494–1529.
- [18] J Zhao, P K Wong, X Ma, et al. Chassis integrated control for active suspension, active front steering and direct yaw moment systems using hierarchical strategy. *Vehicle System Dynamics*, 2017, 55(1): 72–103.
- [19] N Ding, S Taheri. An adaptive integrated algorithm for active front steering and direct yaw moment control based on direct Lyapunov method. *Vehicle System Dynamics*, 2010, 48(10): 1193–1213.
- [20] J Liang, Y Lu, G Yin, et al. A distributed integrated control architecture of AFS and DYC based on MAS for distributed drive electric vehicles. *IEEE Transactions on Vehicular Technology*, 2021, 70(6): 5565–5577.
- [21] Z Shuai, H Zhang, J Wang, et al. Combined AFS and DYC control of four-wheel-independent-drive electric vehicles over CAN network with time-varying delays. *IEEE Transactions on Vehicular Technology*, 2013, 63(2): 591–602.
- [22] X Jin, Z Yu, G Yin, et al. Improving vehicle handling stability based on combined AFS and DYC system via robust Takagi-Sugeno fuzzy control. *IEEE Transactions on Intelligent Transportation Systems*, 2017, 19(8): 2696–2707.
- [23] H Zhang, J Wang. Vehicle lateral dynamics control through AFS/DYC and robust gain-scheduling approach. *IEEE Transactions on Vehicular Technology*, 2015, 65(1): 489–494.
- [24] H Zhang, X Zhang, J Wang. Robust gain-scheduling energy-to-peak control of vehicle lateral dynamics stabilization. *Vehicle System Dynamics*, 2014, 52(3): 309–340.
- [25] W Sun, H Gao, O Kaynak. Adaptive backstepping control for active suspension systems with hard constraints. *IEEE/ASME Transactions on Mechatronics*, 2012, 18(3): 1072–1079.
- [26] Y Qin, Z Wang, K Yuan, et al. Correction to: Comprehensive analysis and optimization of dynamic vibration-absorbing structures for electric vehicles driven by in-wheel motors. *Automotive Innovation*, 2019, 2: 254–262.
- [27] M Hua, G Y Chen, B Y Zhang, et al. A hierarchical energy efficiency optimization control strategy for distributed drive electric vehicles. *Proceedings of the Institution of Mechanical Engineers, Part D: Journal of Automobile Engineering*, 2019, 233(3): 605–621.
- [28] J Liang, J Feng, Z Fang, et al. An energy-oriented torque-vector control framework for distributed drive electric vehicles. *IEEE Transactions on Transportation Electrification*, 2022, DOI: <https://doi.org/10.1109/TTE.2022.3231933>.
- [29] P Wang, H Liu, L Guo, et al. Design and experimental verification of real-time nonlinear predictive controller for improving the stability of production vehicles. *IEEE Transactions on Control Systems Technology*, 2020, 29(5): 2206–2213.
- [30] J Ji, A Khajepour, W W Melek, et al. Path planning and tracking for vehicle collision avoidance based on model predictive control with multiconstraints. *IEEE Transactions on Vehicular Technology*, 2016, 66(2): 952–964.
- [31] G Wang, Y Liu, S Li, et al. New integrated vehicle stability control of active front steering and electronic stability control considering tire force reserve capability. *IEEE Transactions on Vehicular Technology*, 2021, 70(3): 2181–2195.
- [32] Y Song, H Shu, X Chen, et al. Direct-yaw-moment control of four-wheel-drive electrical vehicle based on lateral tyre-road forces and sideslip angle observer. *IET Intelligent Transport Systems*, 2019, 13(2): 303–312.
- [33] B Zhang, S Lu, W Xie. Cooperative game-based driver assistance control for vehicles suffering actuator faults. *IEEE Transactions on Intelligent Transportation Systems*, 2021, 23(7): 8114–8125.
- [34] J Liang, Y Lu, D Pi, et al. A decentralized cooperative control framework for active steering and active suspension: Multi-agent approach. *IEEE Transactions on Transportation Electrification*, 2021, 8(1): 1414–1429.
- [35] B Kapernick, K Graichen. The gradient based nonlinear model predictive control software GRAMPc. *2014 European Control Conference (ECC), Strasbourg, France*, 2014: 1170–1175.

Jiwei Feng born in 1992, is currently a PhD candidate at *School of Mechanical Engineering, Southeast University, China*. His research interests include vehicle dynamics and control, vehicle safety assistance system.

Jinhao Liang born in 1994, is currently a PhD candidate at *School of Mechanical Engineering, Southeast University, China*. He received his bachelor degree from *Nanjing University of Science and Technology, China*, in 2017. His research interests include vehicle dynamics and control, vehicle safety assistance system and connected vehicles.

Yanbo Lu born in 1995, is currently a PhD candidate at *School of Mechanical Engineering, Southeast University, China*. He received his bachelor degree from *Nanjing University of Aeronautics and Astronautics, China*, in 2017. His research interests include vehicle dynamics and control, vehicle rollover prevention.

Weichao Zhuang born in 1990, is currently an assistant professor at *School of Mechanical Engineering, Southeast University, China*. His research interests include vehicle dynamics and control, optimal

control, clean energy vehicles, connected vehicles, and multi-agent control.

Dawei Pi born in 1983, is currently a professor at *School of Mechanical Engineering, Nanjing University of Science and Technology, China*. He received his PhD degree from *Southeast University, China*, in 2010. His research interests include vehicle system dynamics, intelligent control for electric vehicles and intelligent fault-tolerant control of electro-mechanical systems.

Guodong Yin born in 1976, is currently a professor at *School of Mechanical Engineering, Southeast University, China*. He received his PhD degree from *Southeast University, China*, in 2007. His research interests include vehicle dynamics and control, automated vehicles, and connected vehicles.

Liwei Xu born in 1986, is currently an assistant professor at *School of Mechanical Engineering, Southeast University, China*. He received his PhD degree from *Southeast University, China*, in 2020. His research

interests include vehicle dynamics and control, and automated vehicles.

Pai Peng born in 1993, is currently a PhD candidate at *School of Mechanical Engineering, Southeast University, China*. He received his M.S. degree from *Nanjing University of Science and Technology, China*, in 2019. His research interests include connected vehicles and deep learning.

Chaobin Zhou born in 1983, is currently a PhD candidate at *School of Mechanical Engineering, Southeast University, China*. His research interests include vehicle dynamics and control, vehicle active suspension system.